## Composites & nanocomposites

# Effective removal of Cr(VI) from solution by three-dimensional polyaniline loaded composite porous hydrogel

Xuejiao Zhang[1], Wenjie Zou[1], and Jun Chen[1,*]

[1] *School of Chemistry and Chemical Engineering, Anhui University of Technology, Ma Xiang Road, Ma'anshan 243000, People's Republic of China*

## ABSTRACT

It is still challenging to avoid polyaniline agglomeration and fabricate polyaniline-based adsorbents with stable structure, excellent adsorption performance. Herein, we synthesized montmorillonite/humic acid/polyvinyl alcohol@polyaniline (MMT/HA/PVA@PANI) composite porous hydrogel adsorbent by Pickering emulsion template-in situ chemical oxidative polymerization, and the enhancement effect of this design idea on the adsorption performance of PANI was studied with heavy metal ion hexavalent chromium Cr(VI) as the target adsorbate. The in-situ polymerization of aniline at the Pickering emulsion interface and the unique three-dimensional network structure of the hydrogel act as an effective "confinement" for the growth of the polyaniline. The porous structure of hydrogel can be used as water channel, which can accelerate the combination of adsorbate and adsorption site, and significantly improve the adsorption capacity and adsorption rate. Compared with the pure PANI (43.48 mg g$^{-1}$ PANI), MMT/HA/PVA@PANI (1753.60 mg g$^{-1}$ PANI) obviously had significantly higher removal efficiency, which increased the removal efficiency of Cr(VI) by about 40 times. Adsorption experiments suggest that solution pH, adsorbent dosage, contact time and initial concentration all have certain effects on adsorption performance. According to the FESEM, EDX, FTIR and XPS analysis of the materials before and after adsorption, the removal of Cr(VI) is mainly enhanced by ion exchange, electrostatic attraction and chemical reduction. In conclusion, MMT/HA/PVA@PANI adsorbent has novel design, good adsorption performance and strong stability, and it has great development prospects in removing heavy metal ions from wastewater.

## Introduction

Polyaniline (PANI) is a traditional conductive polymer, which has been used as adsorbent for wastewater treatment because of its large number of amine and imine functional groups in the structure [1, 2]. As an adsorbent, PANI has the advantages of easy preparation, low price, easy protonation, easy doping/dedoping and good thermal stability [3, 4]. Benzene (reduction unit)-quinone (oxidation unit) structures coexist in polyaniline, which are in different degrees of redox state with the change of the content of the two structural units, and can be transformed into each other [5]. Therefore, PANI can be used as adsorbent and reducing agent to treat heavy metal ions in water at the same time. PANI is a very potential adsorption material. However, polyaniline is generally polymerized in powder form, which is difficult to process, with small specific surface area and poor mechanical strength, and its effect in practical wastewater treatment is not ideal [6, 7]. PANI-based composite hydrogel is one of the means to solve the above problems. There have been many studies on the removal of heavy metal ionsfrom water by polyaniline composite hydrogel. For example, Galunin et al. [8] prepared a PANI modified hybrid graphene aerogel nanocomposites to purify aquatic media from toxic Pb(II). Ayad et al. [9] synthesized a macroporous PANI/poly (vinyl alcohol) aerogel as adsorbent and reducing agent for Cr(VI) in aqueous solution. PANI composite hydrogel can exert the advantages of PANI and hydrogel synergistically, and is the preferred adsorbent for adsorbing heavy metal ions.

Polyvinyl alcohol (PVA) is a commonly used polymer for preparing hydrogel adsorbents, which is non-toxic and has good hydrophilicity, biocompatibility and chemical–mechanical stability [10, 11]. PVA hydrogel can be crosslinked to form a hydrophilic three-dimensional network structure, which contains rich active hydroxyl groups [12, 13]. PVA as a carrier compounded with PANI can provide a uniform dispersion system, prevent PANI from agglomeration, and improve its adsorption performance, mechanical strength and processability. In addition, the porous nature of PVA hydrogel can not only improve the adsorption capacity but also accelerate the adsorption rate. Pickering emulsion template method is a new strategy to prepare porous hydrogel. Pickering emulsion is an emulsion stabilized by particles, and the particles form a new interfacial layer at the water–oil interface. The solid–liquid interface is very stable because its interface energy is lower than that of the liquid–liquid interface [14, 15]. Pickering emulsion has become an excellent template for producing various porous hydrogels because of its strong anticoalescence, long-term stability, biocompatibility and adjustability [16]. Importantly, the stability and droplet size of Pickering emulsion can be adjusted by solid particles [17]. Clay, as a solid particle with colloidal size, large reserves and low cost, has great advantages in stabilizing Pickering emulsion [18]. Montmorillonite (MMT) is a typical natural clay, which is composed of double-layer siloxane tetrahedron and single-layer alumina octahedron. It has unique cation exchange characteristics, large surface area and high absorption capacity, and has a certain ability to absorb heavy metal ions [19, 20]. However, MMT is very hydrophilic and cannot be stably adsorbed on the oil–water interface, so it needs to be modified to become a suitable stabilizer for Pickering emulsion particles [21, 22].

Water pollution has always been a difficult problem of international concern, especially heavy metal ion pollution. Hexavalent chromium Cr(VI) is a typical heavy metal pollutant, which generally exists in the form of chromate ($CrO_4^{2-}$), hydrogen chromate ($HCrO_4^-$) and dichromate ($CrO_7^{2-}$)in the wastewater discharged from electroplating, anticorrosive coatings, textile printing and dyeing, leather tanning and other industries [23–25]. Cr(VI) is toxic and carcinogenic, and can enter the human body through digestion, respiratory tract, skin and mucous membrane, causing vomiting, abdominal pain, ulcer and liver/kidney function damage. More seriously, long-term or short-term exposure is carcinogenic [26, 27]. Therefore, Cr(VI) must be removed from wastewater before it is discharged into the natural environment to prevent environmental and human health risks.

Herein, MMT/HA/PVA Pickering emulsion was prepared with MMT/HA composite colloidal particle stabilizer obtained by modifying MMT with humic acid (HA). There are a lot of negative charges at the interface of emulsion droplets, which can generate electrostatic attraction with positively charged nitrogen-containing groups in aniline, and aniline can be polymerized in situ at the interface of emulsion droplets through oxidative polymerization. Then, PVA was crosslinked by freeze–thaw cycle [28] to form hydrogel with three-dimensional network structure. Finally, MMT/HA/PVA@PANI composite porous aerogel was obtained by solvent evaporation-freeze drying

(Fig. 1). MMT/HA/PVA @PANI was used as adsorbent to remove Cr(VI) from wastewater, and the effects of adsorption kinetics, adsorption isotherm, solution pH and adsorbent dosage on adsorption performance were systematically studied. At the same time, the structure of the adsorbent before and after adsorption of Cr(VI) was characterized by field emission scanning electron microscope, X-ray energy spectrum, infrared spectrum and X-ray photoelectron spectrum to study the possible adsorption mechanism. This work provides a new way and theoretical reference for efficient utilization of polyaniline and effective removal of Cr(VI) from wastewater.

## Experimental

### Materials

Montmorillonite (MMT) was purchased from Nanocor Company of America. Humic acid (HA) was purchased from houma Jiayou Humic Acid Co., Ltd. Polyvinyl alcohol (PVA) with the average polymerization degree is $1750 \pm 50$, degree of alcoholysis is 99.0%, cyclohexane ($C_6H_{12}$), potassium dichromate ($K_2Cr_2O_7$), aniline ($C_6H_7N$), acetone ($C_3H_6O$), 1,5-diphenylcarbazide, phosphoric acid ($H_3PO_4$), sulfuric acid ($H_2SO_4$), ammonium persulfate (APS) (($NH_4$)$_2S_2O_8$), hydrochloric acid (HCl), sodium hydroxide (NaOH) and ethanol ($C_2H_6O$) are purchased from Sinopharm Chemical Reagents Co., Ltd.(Shanghai, China).

Deionized water (all solutions are prepared from deionized water).

### Synthesis of MMT/HA/PVA@PANI

The MMT/HA/PVA@PANI composite adsorbent was prepared by Pickering emulsion template method-in-situ oxidative polymerization method. Typically, 0.0064 g of humic acid (HA) is dissolved in 0.5 mol L$^{-1}$ NaOH aqueous solution (HA is only dissolved in alkaline aqueous solution) to obtain a sodium humate (NaHA) solution with pH = 11. Then, 0.064 g of montmorillonite (MMT) was added, stirred for 10 min and ultrasonicated to obtain a uniform MMT/NaHA solution. 3.2 mL hydrochloric acid solution (5 M) was added dropwise to obtain MMT/HA composite colloidal particle solution. 16 g of 10% polyvinyl alcohol solution (PVA) and 0.128 g of aniline were added in turn, and the water phase was obtained by stirring evenly. Using 61.7 mL cyclohexane as oil phase, it was poured into water phase under high shear to obtain stable oil-in-water Pickering emulsion. In addition, 0.32 g of ammonium persulfate was dissolved in 4 mL of hydrochloric acid solution (0.5 M), which was poured into the Pickering emulsion as an oxidant, slowly stirred until the color was uniform, and allowed to stand for reaction for 12 h. All the above reactions were carried out at room temperature. After polymerization, hydrogel was obtained through five freeze–thaw cycles, and it was washed with deionized water and ethanol to remove oil phase, unreacted monomer and oligomer. Freeze-drying to obtain

**Figure 1** Schematic diagram for the fabrication of MMT/HA/PVA@PANI adsorbent and adsorption of Cr(VI) solution.
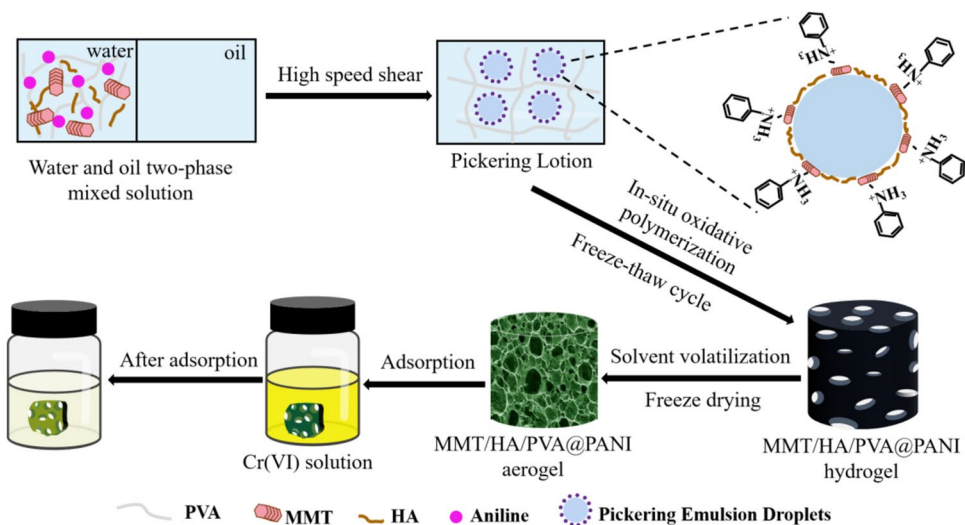
MMT/HA/PVA@PANI composite porous aerogel, and storing for later use. The mass fraction of PANI was determined to be 5.95% due to the weight gain of 0.0633 g per grams of MMT/HA/PVA after introducing PANI.

## Characterization

The droplet stability of Pickering emulsion was confirmed by optical microscope (MOTIC Croup Co., Ltd.), and the droplet size was recorded by taking photos. The elemental composition and micro-morphology of the materials before and after adsorption were measured by field emission scanning electron microscope (FESEM) equipped with energy dispersion analysis system of X-ray spectrometer (EDX) (NOVA Nano SEM 430, FEI Corporation). The functional group changes of PANI, MMT/HA/PVA and MMT/HA/PVA@PANI before and after adsorption were analyzed by Fourier transform infrared spectrometer (FTIR, PerkinElmer, USA). The infrared spectra were recorded in the wave number range of 400–4000 $cm^{-1}$ at room temperature. The X-ray photoelectron spectroscopy (XPS) of MMT/HA/PVA@PANI before and after adsorption were studied by ESCALAB 250XI Xray photoelectron spectrometer (Thermo Fisher) with Al K$\alpha$ radiation (1486.6 eV). The adsorption capacity of MMT/HA/PVA@PANI for Cr(VI) was evaluated by Ultraviolet–visible spectrophotometer (UV3600, shimadzu corporation) in the wavelength range of 500–700 nm.

## Batch adsorption studies

The adsorption performance experiments were carried out in a constant temperature oscillator by batch technology, and the effects of adsorption kinetics, adsorption isotherm, solution pH and adsorbent dosage on the adsorption of Cr(VI) by MMT/HA/PVA@PANI composite adsorbent were studied respectively. The prepared $K_2Cr_2O_7$ stock solution (1000 mg $L^{-1}$) was diluted to prepare Cr(VI) solutions with different concentrations, and the pH value of the solution was adjusted by HCl or NaOH. Typically, the pH of Cr(VI) solution with a concentration of 100 mg $L^{-1}$ was adjusted to 2–10 to analyze the influence of solution pH on adsorption performance. Different doses of adsorbent were added according to the dosage of 0.5–5 g $L^{-1}$ to study the effect of adsorbent dosage. The adsorption kinetics was tested in the adsorption time

range of 0–600 min. The adsorption isotherm experiments were carried out at three temperatures (298, 308, 318 K), and the initial concentration of Cr(VI) solution was in the range of 50–250 mg $L^{-1}$. At the same time, the thermodynamic parameters are analyzed. Three parallel experiments were carried out in all experiments to improve the accuracy of the experiments.

The residual Cr(VI) ion concentration was measured by UV–vis spectrophotometer (UV3600, Shimadzu Corporation) with the help of 1,5-Diphenylcarbazide [29], and converted into concentration value according to standard curve. The removal rate R (%) of adsorbents on Cr(VI) and the adsorbed Cr(VI) amount on per gram of adsorbent $Q_t$ (mg $g^{-1}$) in time t were calculated using Eqs. (1) and (2) as follows [30]:

$$R(\%) = \frac{C_0 - C_t}{C_0} \times 100 \tag{1}$$

$$Q_t = \frac{C_0 - C_t}{m} \times V \tag{2}$$

where $C_0$ (mg $L^{-1}$) and $C_t$ (mg $L^{-1}$) correspond to the initial concentrations of Cr(VI) ions and the residual concentration of Cr(VI) at time t, respectively. m (g) is the mass of adsorbent used, and V (L) is the volume of Cr(VI) solution.

## Results and discussion

### Characterization of MMT/HA/PVA@PANI

The structure and surface morphology of adsorbents are important data for understanding the adsorption process. From Fig. 2a, we can clearly see the structure and size of the droplets. Compared with Fig. 2b, c, it shows that the droplet size of Pickering emulsion is basically consistent with the pore sizes of MMT/HA/PVA and MMT/HA/PVA@PANI composite adsorbents. It is proved that Pickering emulsion stabilized by MMT/HA composite colloidal particles has excellent stability and is a good template for preparing porous hydrogels. Figure 2c shows that MMT/HA/PVA@PANI adsorbents has a large number of micron-sized pores, which can be used as water channels to accelerate the combination of adsorbent and adsorption sites, and improve the adsorption rate. In addition, there is a similar pore structure in MMT/HA/PVA, which shows that the introduction of PANI has not changed the

**Figure 2** Optical microscope images of Pickering emulsion droplets (**a**). Low magnification FESEM images (**b, c**) and high magnification FESEM images (**d, e**) of MMT/HA/PVA and MMT/HA/PVA@PANI. EDX analysis images of MMT/HA/PVA (**f**), MMT/HA/PVA@PANI (**g**). FTIR spectra of PANI, MMT/HA/PVA, MMT/HA/PVA@PANI (**h**).
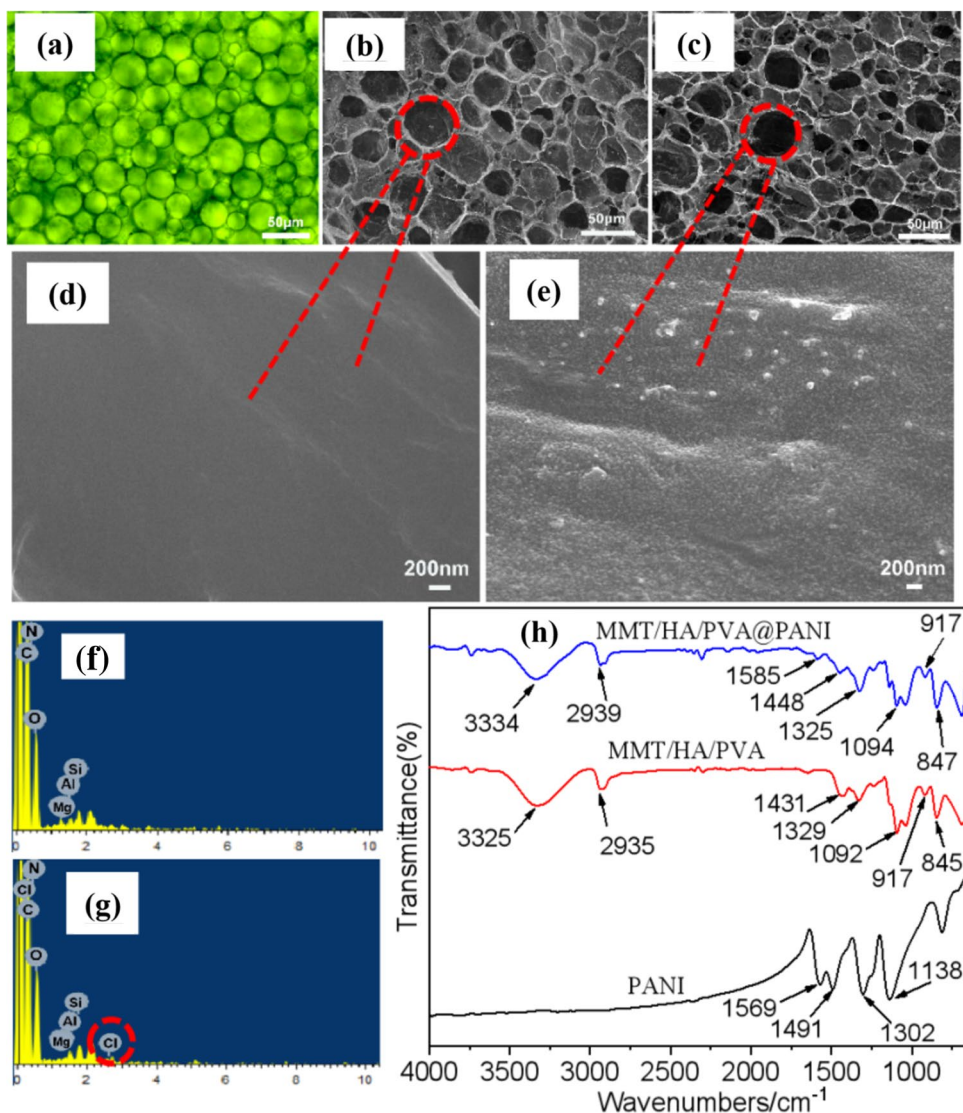


structure of the material. Further compare the high-power SEM images of the materials before and after PANI introduction (Fig. 2d, e), it is noted that the surface of MMT/HA/PVA is smooth, while the surface of MMT/HA/PVA@PANI becomes rough due to covering a large amount of PANI. The results suggested that PANI was successfully compounded on the composite adsorbent, which could effectively avoid the aggregation of PANI and improve its utilization rate. Therefore, it can be considered that MMT/HA/PVA@PANI has great potential in adsorbing Cr(VI). The EDX elements of MMT/HA/PVA and MMT/HA/PVA@PANI were analyzed, and the results are shown in Fig. 2f, g. It is found that carbone (C), nitrogen (N), oxygen (O), aluminum (Al), silicon (Si) and magnesium (Mg) are the main elements of MMT/HA/PVA, while MMT/HA/

PVA@ PANI adds chlorine (Cl) element, which comes from the Cl doping of PANI [31]. EDX confirmed the successful compounding of PANI and MMT/HA/PVA.

Figure 2h shows the infrared spectrum analysis results of PANI, MMT/HA/PVA and MMT/HA/PVA @PANI. The PANI curve has the following characteristic peaks [32, 33], which correspond to the stretching vibration peak of quinone ring skeleton (1491 cm$^{-1}$), the bending vibration of C–H bond in benzene ring plane (1138 cm$^{-1}$), the absorption peak of C=C on benzene ring (1569 cm$^{-1}$) and the stretching vibration of C–N (1302 cm$^{-1}$). For MMT/HA/PVA curve, the tensile vibration peak of Si–O bond is 1092 cm$^{-1}$, the deformation vibration peak of OH bond is 845 cm$^{-1}$, and the bending vibration peak of Al–OH bond is 917 cm$^{-1}$. These peaks all come from MMT [34] in the material.

The C–C tensile vibration peak at 1431 cm$^{-1}$, CH– tensile vibration peak at 2935 cm$^{-1}$ and –OH tensile vibration peak at 3325 cm$^{-1}$ can belong to PVA [35]. In the MMT/HA /PVA@PANI curve, some characteristic peaks of PANI and MMT/HA/PVA obviously exist, which proves that PANI and MMT/HA/PVA have been successfully compounded. It is worth noting that the nitrogen-containing functional groups that play a major role in Cr(VI) adsorption also remain in the composite adsorbent.

## Sorption enhancement of Cr(VI) from aqueous solution by PANI loaded on the hydrogel

Using Cr(VI) as the target adsorbent, the enhancement effect of PANI's actual adsorption efficiency in MMT/HA/PVA@PANI was evaluated. According to the proportion of PANI and MMT/ HA/PVA in MMT/HA/PVA@PANI, the actual adsorption amount of Cr(VI) by PANI can be calculated. The detailed data are listed in Table 1. Obviously, the adsorption capacity of MMT/HA/PVA (44.02 mg g$^{-1}$) and the pure PANI in reference [5] (43.48 mg g$^{-1}$) is much lower than that of MMT/HA/PVA@PANI (145.74 mg g$^{-1}$) in this experiment. Moreover, according to the mass fraction of PANI and MMT/HA/PVA in MMT/HA@PANI, the

adsorption capacity of MMT/HA@PANI for Cr(VI) can reach 1753.60 mg g$^{-1}$ PANI, which is 40 times higher than that of pure PANI (43.48 mg g$^{-1}$ PANI). It is clarified that MMT/HA/PVA@PANI can effectively avoid the agglomeration of PANI to improve the adsorption performance of Cr(VI), and can be used as an effective adsorbent for removing Cr(VI) from water.

## Effect of pH

One of the indispensable conditions for understanding the adsorption performance of adsorbents is the solution pH, because the solution pH will directly affect the existing form of Cr(VI) ions in aqueous solution and the surface charge of adsorbents. In this experiment, the change of Cr(VI) adsorption capacity of MMT/HA/PVA@PANI at different solution pH was investigated by adjusting the pH from 2 to 10, and the results are shown in Fig. 3a. In addition, the distribution of the existing forms of Cr(VI) at different pH values was plotted in Fig. 3b [36]. As can be seen from Fig. 3a, the maximum adsorption capacity is at pH 2, and then the adsorption capacity decreases rapidly with the increase of pH value of the solution, which corresponds to Fig. 3b. Figure 3b shows that in the pH range of 2–6, the main form of Cr(VI) ion is $Cr_2O_7^{2-}$ or $HCrO_4^-$. At this time, the degree of amino protonation of MMT/HA/PVA@ PANI adsorbent is high, which leads to a significant increase in the surface positive charge, and the negatively charged Cr(VI) anion is turn adsorbed by electrostatic attraction. On the other hand, the Cl$^-$ doped on PANI can be replaced by $Cr_2O_7^{2-}$ or $HCrO_4^-$ under acidic conditions, and adsorb Cr(VI) anion by ion exchange [29]. In contrast, in aqueous solution with pH > 6, $CrO_4^{2-}$ becomes the dominant

**Table 1** Comparison of adsorption capacity of different samples

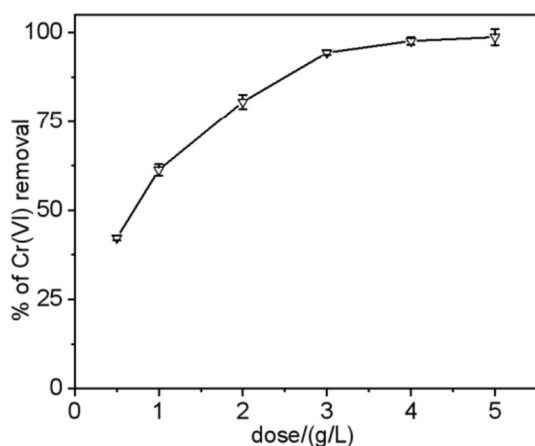| Sample | PANI content (%) | $q_e$ (mg g$^{-1}$) | Unit PANI adsorption capacity (mg g$^{-1}$) |
|---|---|---|---|
| MMT/HA/PVA | 0 | 44.02 | 0 |
| PANI [5] | 100 | 43.48 | 43.48 |
| MMT/HA/PVA@ PANI | 5.95 | 145.74 | 1753.60 |

**Figure 3** Effect of solution pH on adsorption performance (**a**) and species distribution of Cr(VI) at different pH (**b**) ($C_0 = 100$ mg L$^{-1}$, t = 12 h, T = 298 K, adsorbent dosage = 1 g L$^{-1}$).
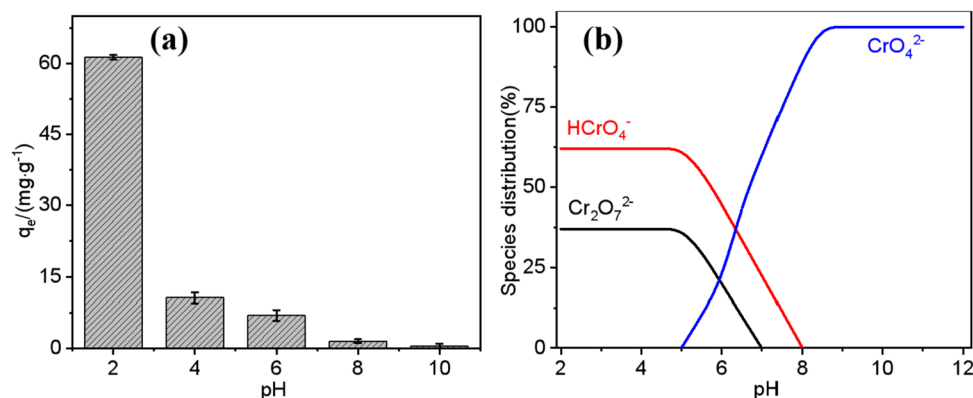
form of Cr(VI). The increase of solution pH results in the decrease of positive charge on the surface of adsorbent due to deprotonation of amino group, and the electrostatic repulsion between Cr(VI) anion and adsorbent increases, thus limiting the adsorption of Cr(VI). Furthermore, $OH^-$ in solution may compete with $CrO_4^{2-}$ for adsorption sites, which will further reduce the adsorption capacity of materials [31].

## Effect of adsorbent dose

The dosage of adsorbent is also an important parameters for evaluating the performance of adsorbent. In this experiment, different doses of adsorbent were added according to the dosage of 0.5–5 g $L^{-1}$ to investigate the effect of adsorbent dosage on Cr(VI) adsorption. Figure 4 shows that the removal rate of Cr(VI) varies with the increase of adsorbent dosage. Obviously, with the increase of dosage, the removal rate of Cr(VI) by MMT/HA/PVA@ PANI also increased, and the removal rate increased slowly after reaching 80.6%. When the dosage is further increased to 5 g $L^{-1}$, the removal rate of Cr(VI) reaches 98.77%. In the process of increasing from 0.5 g $L^{-1}$ to 1 g $L^{-1}$, it is speculated that the increase of Cr(VI) removal rate is justified by the increase of effective adsorption sites. With the increasing amount of adsorbent, the concentration of Cr(VI) is relatively reduced, and the driving force to overcome the solid–liquid mass transfer resistance is also
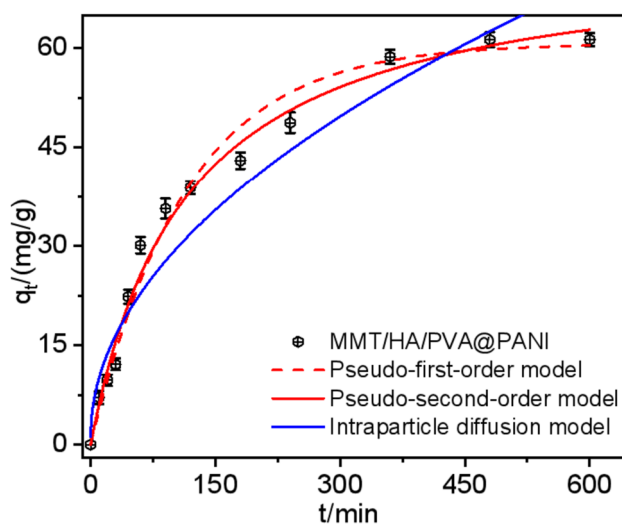
reduced, so the increase of adsorption rate slows down.

## Adsorption kinetics

The adsorption reaction time also has a significant effect on the removal of Cr(VI). Within that range of 0–600 min, the effect of adsorption time on the adsorption of Cr(VI) on MMT/HA/PVA@ PANI composite is shown in Fig. 5. During the 0–60 min adsorption process, the adsorption capacity increased rapidly with the increase of reaction time, because there were a large number of available adsorption active sites on the adsorbent at the initial stage of the reaction, and the concentration of Cr(VI) in the local micro-environment of adsorbent-adsorbate was high. In the later stage of adsorption reaction, most of the adsorption active sites are occupied by Cr(VI), and the concentration of Cr(VI) in the local micro-environment of adsorbent-adsorbate is also decreasing, which leads to the slow increase of adsorption rate to equilibrium in the later stage.

Pseudo-first-order model and pseudo-second-order model [37] were used for nonlinear fitting of experimental data to understand the adsorption kinetics of MMT/HA/PVA@PANI. Moreover, the intraparticle diffusion model [38] was adopted to further study the diffusion mechanism of Cr(VI) on MMT/HA/PVA@ PANI adsorbent. The nonlinear equations of the three models are as follows:



**Figure 4** Effect of adsorbent dosage on adsorption performance ($C_0 = 100$ mg $L^{-1}$, pH = 2, t = 12 h, T = 298 K).



**Figure 5** Kinetics of MMT/HA/PVA@PANI adsorption of Cr(VI) ($C_0 = 100$ mg $L^{-1}$, T = 298 K, adsorbent dosage = 1 g $L^{-1}$, pH = 2).

Pseudo – first – order: $\quad q_t = q_e\left(1 - e^{-k_1 t}\right)$ $\qquad$ (3)

Pseudo – second – order: $\quad q_t = \dfrac{k_2 q_e^2 t}{1 + k_2 q_e t}$ $\qquad$ (4)

Intraparticle diffusion model: $\quad q_t = k_3 t^{0.5} + C$ $\qquad$ (5)

where $k_1$ (min$^{-1}$) and $k_2$ [g (mg min)$^{-1}$] are pseudo-first-order and pseudo-second-order rate constants respectively, $q_t$ (mg g$^{-1}$) is the amount of Cr(VI) adsorbed at time t, $q_e$ (mg g$^{-1}$) is equilibrium adsorption amount, $k_3$ [mg (g min$^{-0.5}$)$^{-1}$] is the particle diffusion constant, and C is the boundary layer thickness constant. The kinetic fitted plots is shown in Fig. 5, and the kinetic parameters are summarized in Table 2. As demonstrated, the pseudo-second-order model is more suitable to describe the adsorption of Cr(VI) on MMT/HA/PVA@PANI, because its correlation coefficient ($R^2 = 0.991$) is closer to 1, and the calculated adsorption amount $q_e$ (74.75 mg g$^{-1}$) is closer to the experimental value $q_e$ (80.08 mg g$^{-1}$). Therefore, it can be considered that the adsorption of Cr(VI) is mainly a chemical reaction, and electron exchange (redox reaction) may occur between adsorbent and adsorbate [39]. According to the intraparticle diffusion diagram (Fig. 5) and fitting parameters (Table 2), the correlation coefficient $R^2$ is 0.948, the fitting curve does not pass through the coordinate origin, and the value of the boundary layer thickness constant C is not 0, which indicates that intraparticle diffusion is an important rate control factor in the adsorption process of Cr(VI), but it is not the only decisive factor, and it can be

inferred that intraparticle diffusion and membrane diffusion go on together in the adsorption process [40].

## Adsorption isotherm

In order to know the interaction between adsorbate and adsorbent and determine the maximum adsorption capacity, Langmuir model (single-layer homogeneous adsorption) and Freundlich model (multi-layer heterogeneous adsorption) [44] were used to fit the experimental data. The nonlinear equations of the two models are as follows:

Langmuir: $\quad q_e = \dfrac{K_L q_m C_e}{1 + K_L C_e}$ $\qquad$ (6)

Freundlich: $\quad q_e = K_F C_e^{1/n}$ $\qquad$ (7)

where $C_e$ (mg L$^{-1}$) is the Cr(VI) mass concentration in solution equilibrium, $q_e$ (mg g$^{-1}$) is equilibrium adsorption amount, $q_m$ (mg g$^{-1}$) is the maximum adsorption capacity, $K_L$ (L mg$^{-1}$) is the Langmuir constant related to adsorption energy, $K_F$ (mg g$^{-1}$) and n are Freundlich isotherm parameters related to adsorption capacity and adsorption strength respectively. From Fig. 6a, the adsorption capacity of MMT/HA/PVA@PANI increases with the increase of initial concentration of Cr(VI) in the solution, and then tends to balance gradually. Probably because there are a lot of empty adsorption sites on the adsorbent at at the beginning, Cr(VI) in the solution will quickly occupy the adsorption site as soon as it comes into contact with the adsorbent, and the adsorption capacity will increase rapidly. Nevertheless, with the continuous increase of Cr(VI) concentration, the limited adsorption sites have gradually been completely occupied, and the adsorption capacity tends to be balanced. Additionally, the adsorption capacity increases with the increase of temperature, and reaches the maximum adsorption capacity of 145.74 mg g$^{-1}$ at 318 K, which indicates that the temperature is positively correlated with the adsorption performance of the material, and the adsorption process of the material is an endothermic reaction process.

The fitting curve of adsorption isotherm model and the calculated model parameters are shown in Fig. 6 and Table 3. For MMT/HA/PVA@PANI, it is obvious that Langmuir model fitted well to the sorption data of Cr(VI), and the correlation coefficient $R^2$ is higher, indicating that Langmuir model is more suitable for

**Table 2** Adsorption kinetic models and parameters for removal of Cr(VI) on MMT/HA/PVA@PANI

| Kinetic models | Parameters | |
|---|---|---|
| Pseudo-first-order | $C_0$ (mg L$^{-1}$) | 100 |
| | $q_e$(exp) (mg g$^{-1}$) | 80.08 |
| | $k_1$ (min$^{-1}$) | 0.020 |
| | $q_e$ (mg g$^{-1}$) | 60.71 |
| | $R^2$ | 0.988 |
| Pseudo-second-order | $k_2$ [g (mg min)$^{-1}$] | 0.0002 |
| | $q_e$ (mg g$^{-1}$) | 74.75 |
| | $R^2$ | 0.991 |
| Intraparticle diffusion | $k_3$ [mg (g min$^{-0.5}$)$^{-1}$] | 2.801 |
| | C | 1.164 |
| | $R^2$ | 0.948 |

**Figure 6** Isotherm of MMT/ HA/PVA@PANI adsorption of Cr(VI) (pH = 2, adsorbent dosage = 1 g L$^{-1}$, t = 12 h).
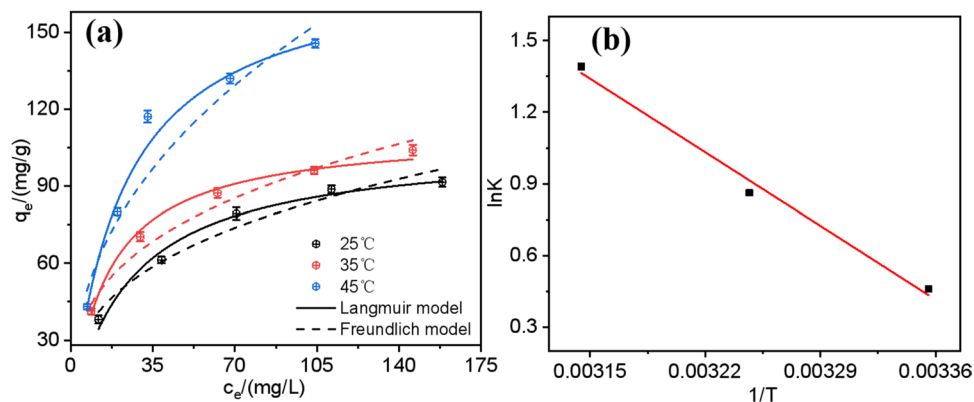


**Table 3** Adsorption isotherm models and parameters for removal of Cr(VI) on MMT/HA/PVA@PANI

| Isotherm models | Parameters | Temperature (K) | | |
| --- | --- | --- | --- | --- |
| | | 298 | 308 | 318 |
| Langmuir | $q_m$ (mg g$^{-1}$) | 106.30 | 111.21 | 176.77 |
| | $K_L$ (L mg$^{-1}$) | 0.040 | 0.064 | 0.045 |
| | $R^2$ | 0.981 | 0.994 | 0.991 |
| Freundlich | $K_F$ (mg g$^{-1}$) | 18.01 | 22.06 | 21.99 |
| | $1/n$ | 0.332 | 0.319 | 0.417 |
| | $R^2$ | 0.974 | 0.981 | 0.958 |

describing the adsorption process of Cr(VI) by MMT/ HA/PVA@PANI than Freundlich model. The results show that the adsorption of Cr(VI) on the composite is mainly monolayer adsorption, and the active sites are evenly distributed on the adsorbent [45]. Remarkably, with the temperature rising from 298 to 318 K, the maximum adsorption capacity $q_m$ calculated by Langmuir model increased from 106.3 to 176.77 mg g$^{-1}$, which indicated that increasing the temperature was beneficial to the adsorption reaction, and it was speculated that the adsorption mechanism might be mainly chemical interaction rather than physical interaction.

Table 4 lists the maximum adsorption capacity of various PANI-based adsorbents reported in the literature for Cr(VI) removal, from which we can see that the adsorption capacity of the MMT/HA/PVA @PANI composite material studied in this experiment is higher than that of most literature adsorbents, indicating that MMT/HA/PVA@PANI composite may be considered as a promising adsorbent that can be used to remove Cr(VI) from aqueous solutions.

## Thermodynamics studies

The adsorption of Cr(VI) on MMT/HA/PVA@PANI (initial concentration is 100 mg L$^{-1}$) was analyzed by thermodynamics. Thermodynamic parameters such as standard Gibbs free energy change ($\Delta G^0$), enthalpy change ($\Delta H^0$) and entropy change ($\Delta S^0$) are calculated by the following equation [43]:

$$\ln K = \frac{\Delta S^0}{R} - \frac{\Delta H^0}{RT} \tag{8}$$

$$\Delta G^0 = -RT \ln K \tag{9}$$

**Table 4** Comparison of Cr(VI) removal capacity using MMT/HA/PVA@ PANI with other PANI-based adsorbents

| Adsorbents | $q_m$ (mg g$^{-1}$) | pH | Initial Cr(VI) concentration (mg L$^{-1}$) | References |
| --- | --- | --- | --- | --- |
| Exfoliated graphite/Polyaniline composite | 38.2 | 7 | 150–350 | [41] |
| Polystyrene/Polyaniline-Fe$_3$O$_4$ | 25.189 | 2 | 10–40 | [42] |
| Polyaniline@nanoparticles-600 nanocomposites | 198.04 | 1 | 40–160 | [43] |
| Polyaniline/Poly(vinyl alcohol) aerogels | 41.2 | 2 | 13–50 | [9] |
| MMT/HA/PVA@PANI | 145.74 | 2 | 50–250 | This study |

$$K = \frac{C_0 - C_e}{C_e} \qquad (10)$$

where K (L g$^{-1}$) is thermodynamic equilibrium constant, R [8.314 J (mol K)$^{-1}$] is the ideal gas constant, T (K) is temperature in Kelvin, $C_0$ (mg L$^{-1}$) is the initial concentrations of Cr(VI) ions and $C_e$ (mg L$^{-1}$) is the Cr(VI) mass concentration in solution equilibrium. The values of $\Delta H^0$ and $\Delta S^0$ come from the slope and intercept of lnK-1/T diagram (Fig. 6b). The thermodynamic parameters obtained are shown in Table 5. At all experimental temperatures, $\Delta G^0$ is negative, indicating that the adsorption process of Cr(VI) is spontaneous, and the greater the negative value of $\Delta G^0$, the better the adsorption [6]. The values of $\Delta G^0$ in Table 5 are −3.92, −6.06 and −10.63 kJ mol$^{-1}$ respectively, and the negative values increase with the increase of temperature, which confirms that high temperature is beneficial to adsorption. In addition, the positive value of $\Delta H^0$ proves that the adsorption process is endothermic, which further proves that high temperature will promote the adsorption of Cr(VI), and also supports the discussion results of isotherm model. The positive value of $\Delta S^0$ implies that the randomness of solid–liquid interface increases during adsorption [46]. This is consistent with the results of kinetic research.

## Adsorption mechanism

The FESEM, EDX, FTIR and XPS of the adsorbent before and after adsorption were determined to study the possible adsorption mechanism of Cr(VI) on MMT/HA/PVA@PANI composite adsorbent. Figure 7a, b show the low and high magnification FESEM images of MMT/HA/PVA@PANI after Cr(VI) adsorption. Compared with Figs. 7a, 2c, the adsorbent after adsorption still maintains the porous structure, and the overall structure and pore size are almost the same as those before adsorption, which confirms the

**Table 5** Thermodynamic parameters for removal of Cr(VI) on MMT/HA/PVA@PANI

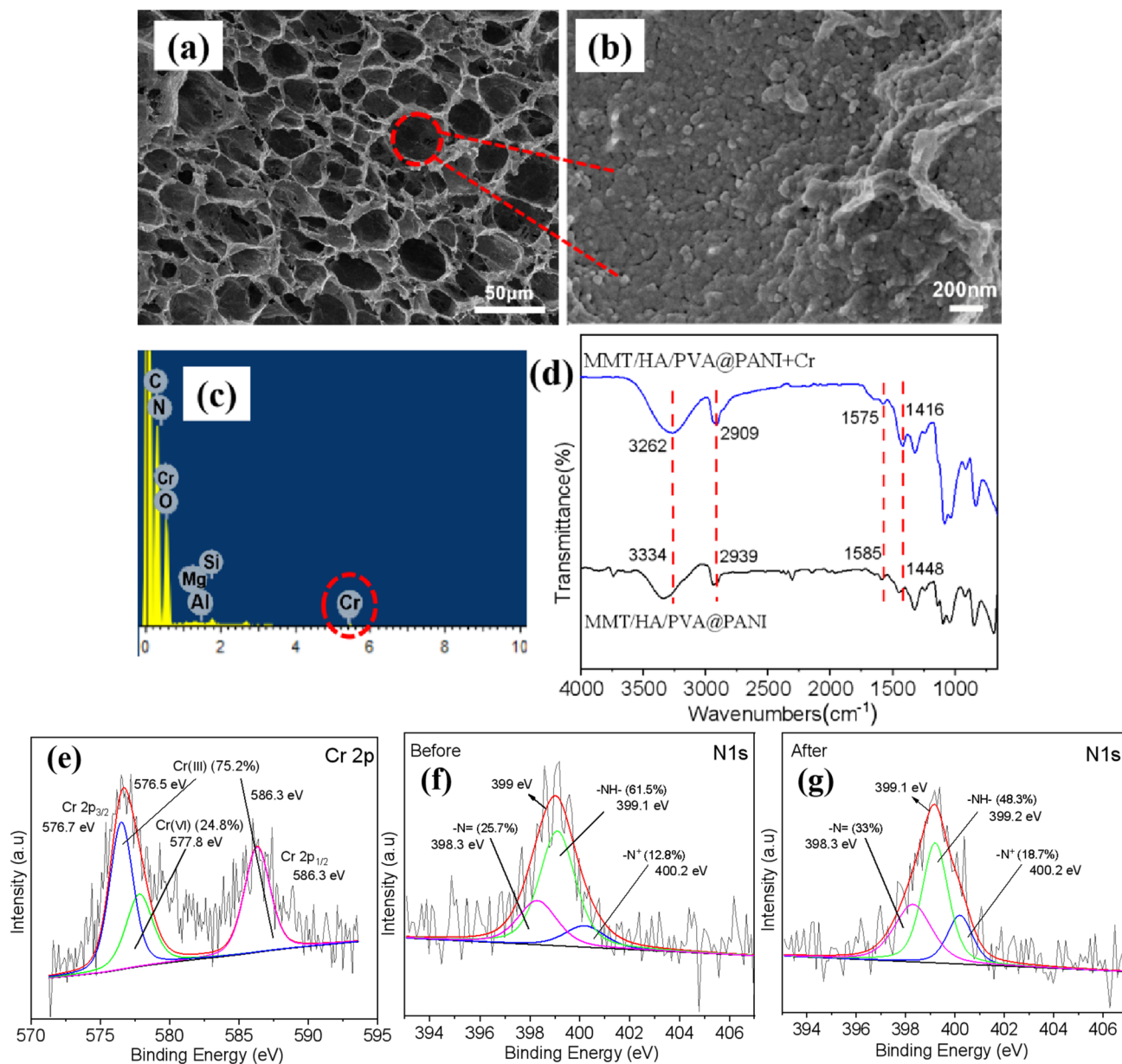| T(K) | Thermodynamic parameters | | |
|------|--------------------------|---|---|
| | $\Delta G^0$ (kJ mol$^{-1}$) | $\Delta H^0$ (kJ mol$^{-1}$) | $\Delta S^0$ [kJ (mol K)$^{-1}$] |
| 298 | − 3.92 | | |
| 308 | − 6.06 | 36.639 | 0.127 |
| 318 | − 10.63 | | |

excellent stability of Pickering emulsion stabilized by MMT/HA composite colloidal particles. Moreover, the results in Fig. 7b are similar to those in Fig. 2e, and there are still a large number of PANI evenly distributed on the rough adsorbent surface, which once again proves that the structure of MMT/HA/PVA@PANI is stable. Figure 7c is the EDX element spectrum of Cr(VI) after adsorption. Compared with Fig. 2g, there is an obvious Cr element peak in the energy spectrum, and the Cl element peak disappears, indicating that the doped Cl$^-$ is substituted and the Cr(VI) anion can be adsorbed by ion exchange [47]. EDX elemental analysis is the direct evidence that MMT/HA/ PVA@ PANI adsorbs Cr(VI).

The possible mechanism of Cr(VI) adsorption was analyzed by observing the change of functional groups. Figure 7d is the FTIR spectrum of MMT/HA/ PVA@PANI before and after adsorbing Cr(VI). It was observed that the shape of the whole infrared spectrum remained basically unchanged after Cr(VI) was adsorbed, and the peak of the whole spectrum shifted slightly to the low wavenumber, indicating that the adsorption reaction did not destroy the structure of the adsorbent. The red shift of spectral peak reflects the interaction between Cr(VI) and adsorbent [48]. Combined with the results of EDX element analysis, it is speculated that the ion exchange between Cr(VI) anion and Cl$^-$ affects the conjugated structure of PANI, limits the delocalization degree of polymer chain, and then leads to the red shift of the peak. It was found that the peaks at 1448 and 1585 cm$^{-1}$ related to the C=N stretching vibration peak of quinone ring skeleton and the C=C stretching vibration peak of benzene ring on PANI shifted to 1416 and 1575 cm$^{-1}$, respectively, which indicated that PANI played a certain role in the adsorption reaction, and the Cr(VI) anion may be adsorbed by positively charged protonated amino groups through electrostatic attraction [32]. Moreover, the tensile vibration peaks of CH− at 3334 cm$^{-1}$ and –OH at 2939 cm$^{-1}$ moved to 3262 and 2909 cm$^{-1}$, indicating that the hydrogel structure as a carrier may also have some adsorption effect on Cr(VI).

The possible mechanism of Cr(VI) adsorption was further investigated in detail by XPS characterization. Figure 7d is the high-resolution XPS spectra of Cr 2p of MMT/HA/PVA@PANI after Cr(VI) adsorption. It is observed that there are two peaks in the spectrum of Cr 2p at 576.7 and 586.3 eV, which can correspond to Cr 2p$_{3/2}$ and Cr 2p$_{1/2}$. These two peaks can be divided into three peaks: 577.8 (Cr 2p$_{3/2}$), 576.5 (Cr 2p$_{3/2}$) and

**Figure 7** Low and high magnification FESEM (**a**, **b**), and EDX (**c**) of MMT/HA/PVA@PANI after Cr(VI) adsorption. FTIR spectra (**d**) of MMT/HA/PVA@PANI before and after Cr(VI) adsorption. High-resolution XPS spectra of Cr 2p (**e**) of MMT/ HA/PVA@PANI after Cr(VI) adsorption. High-resolution XPS spectra of N 1s (**f**, **g**) of MMT/HA/PVA@PANI before and after Cr(VI) adsorption.

586.3 (Cr $2p_{1/2}$) eV. The first peak corresponds to Cr(VI), and the last two peaks correspond to Cr(III). According to the calculation of peak area, about 24.8% of Cr(VI) is on the adsorbent, and another 75.2% has been reduced to Cr(III), which proves that there is redox reaction on the adsorbent [49]. The reduction reaction needs an electron donor, and the amino group in PANI can just serve as an electron donor group to

provide electrons for the reduction of Cr(VI) [50]. Therefore, the N 1s before and after Cr(VI) adsorption was characterized by high-resolution XPS spectrum (Fig. 7f, g). Figure 7f shows that the XPS spectrum of N 1s before adsorption has a peak at 399 eV, which can be deconvolved into three different peaks at 398.3, 399.1 and 400.2 eV, respectively. These three peaks are attributed to 25.7% imine nitrogen (–N=), 61.5%

amine nitrogen (–NH–) and 12.8% charged nitrogen (–N$^+$) groups respectively [33]. –N$^+$ is derived from the protonation of some imines under acidic conditions. After adsorption, the slight changes of peak positions suggests that N-containing functional groups participate in Cr(VI) adsorption reaction. Furthermore, the percentage of nitrogen component in the material has also changed. The proportion of –NH– decreased to 48.3%, while the proportion of –N= increased to 33%, which confirmed that part of –NH– on the adsorbent participated in the reduction reaction of Cr(VI) as an electron donor group [51]. The charged nitrogen (–N$^+$) group can generate electrostatic attraction with Cr(VI) to adsorb Cr(VI). XPS analysis shows that the adsorption mechanism of Cr(VI) may include electrostatic attraction and redox reaction.

Based on the above analysis, the adsorption of Cr(VI) on MMT/HA/PVA@PANI adsorbent is mainly through ion exchange, electrostatic attraction and redox reaction.

## Conclusion

A novel composite porous hydrogel adsorbent MMT/HA/PVA@PANI was successfully prepared by Pickering emulsion template-in-situ oxidative polymerization for adsorption of heavy metal ions hexavalent chromium Cr(VI) in aqueous solution. The adsorption performance of MMT/HA/PVA@ PANI is highly dependent on the solution pH. The adsorption of Cr(VI) by MMT/HA/PVA@PANI is more in line with the pseudo-second-order kinetic model, mainly chemical adsorption. The intraparticle diffusion model infers that the intraparticle diffusion is not the only decisive step, but it is carried out together with membrane diffusion in the adsorption process of MMT/HA/PVA@ PANI. The adsorption behavior of the material is more suitable to be fitted by Langmuir model, which belongs to single-layer homogeneous adsorption. Thermodynamic study suggests that Cr(VI) adsorption is a spontaneous endothermic reaction, and increasing temperature is beneficial to adsorption. Mechanism studies suggested that the adsorption of Cr(VI) on MMT/HA/PVA@PANI adsorbent is mainly through ion exchange, electrostatic attraction and redox reaction. Excitedly, the maximum adsorption capacity of PANI in MMT/HA/PVA@PANI for Cr(VI) can reach 1753.60 mg g$^{-1}$-PANI, which is almost 40 times that of pure PANI (43.48 mg g$^{-1}$). MMT/HA/

PVA@PANI exerts the adsorption potential of PANI significantly, which provides new ideas and technologies for improving the utilization rate of PANI and preparing more efficient Cr(VI) adsorbent.

## Author contributions

All authors contributed to the study conception and design. XZ: process the data and write the manuscript. WZ: complete material preparation, data collection and analysis. JC: corresponding author. Directed, revised, and supplemented the manuscript. All authors commented on previous versions of the manuscript, and all authors read and approved the final manuscript.

## Funding

## Declarations

**Conflict of interest** The authors state that they do not have any established competing financial interests or personal relationships that might seem to have affected the work reported in this article.

**Ethics approval** Not applicable.

**Consent to participate** Not applicable.

**Consent for publication** Not applicable.

## References

[1] Stejskal J (2022) Recent advances in the removal of organic dyes from aqueous media with conducting polymers, polyaniline and polypyrrole, and their composites. Polymers (Basel) 14(19):4243. https://doi.org/10.3390/polym14194243

[2] Stejskal J (2019) Conducting polymers are not just conducting: a perspective for emerging technology. Polym Int 69(8):662–664. https://doi.org/10.1002/pi.5947

[3] Senguttuvan S, Senthilkumar P, Janaki V, Kamala-Kannan S (2021) Significance of conducting polyaniline based composites for the removal of dyes and heavy metals from aqueous solution and wastewaters-a review. Chemosphere 267:129201. https://doi.org/10.1016/j.chemosphere.2020.129201

[4] Wani AA, Khan AM, Manea YK, Salem MAS, Shahadat M (2021) Selective adsorption and ultrafast fluorescent detection of Cr(VI) in wastewater using neodymium doped polyaniline supported layered double hydroxide nanocomposite. J Hazard Mater 416:125754. https://doi.org/10.1016/j.jhazmat.2021.125754

[5] Chen ZS, Wei BB, Yang SY, Li Q, Liu L, Yu SJ, Wen T, Hu BW, Chen JR, Wang XK (2019) Synthesis of PANI/AlOOH composite for Cr(VI) adsorption and reduction from aqueous solutions. ChemistrySelect 4(8):2352–2362. https://doi.org/10.1002/slct.201803898

[6] Javadian H, Ghaemy M, Taghavi M (2013) Adsorption kinetics, isotherm, and thermodynamics of $Hg^{2+}$ to polyaniline/hexagonal mesoporous silica nanocomposite in water/ wastewater. J Mater Sci 49(1):232–242. https://doi.org/10.1007/s10853-013-7697-7

[7] Muhammad A, Shah A, Bilal S (2019) Comparative study of the adsorption of acid blue 40 on polyaniline, magnetic oxide and their composites: synthesis. Charact Appl Mater (Basel) 12(18):2854. https://doi.org/10.3390/ma12182854

[8] Kuznetsova TS, Burakov AE, Burakova IV, Pasko TV, Dyachkova TP, Mkrtchyan ES, Memetova AE, Ananyeva OA, Shigabaeva GN, Galunin EV (2023) Preparation of a polyaniline-modified hybrid graphene aerogel-like nanocomposite for efficient adsorption of heavy metal ions from aquatic media. Polymers (Basel) 15(5):1101. https://doi.org/10.3390/polym15051101

[9] Zaghlol S, Amer WA, Shaaban MH, Ayad MM, Bober P, Stejskal J (2020) Conducting macroporous polyaniline/poly(vinyl alcohol) aerogels for the removal of chromium(VI) from aqueous media. Chem Pap 74(9):3183–3193. https://doi.org/10.1007/s11696-020-01151-z

[10] Song XF, Qin JT, Li TT, Liu G, Xia XX, Li YS, Liu Y (2019) Efficient construction and enriched selective adsorption-photocatalytic activity of PVA/PANI/$TiO_2$ recyclable hydrogel by electron beam radiation. J Appl Polym Sci 137(13):48516. https://doi.org/10.1002/app.48516

[11] Xiao ZX, Zhang LJ, Wu L, Chen D (2019) Adsorptive removal of Cu(II) from aqueous solutions using a novel macroporous bead adsorbent based on poly(vinyl alcohol)/sodium alginate/$KMnO_4$ modified biochar. J Taiwan Inst Chem E 102:110–117. https://doi.org/10.1016/j.jtice.2019.05.010

[12] Song W, Tong TJ, Xu J, Wu N, Ren LL, Li M, Tong J (2022) Preparation and application of green chitosan/ploy(vinyl alcohol) porous microspheres for the removal of hexavalent chromium. Mater Sci Eng B 284:115922. https://doi.org/10.1016/j.mseb.2022.115922

[13] Wang JJ, Chi H, Zhou AA, Zheng RH, Bai H, Zhang TY (2020) Facile synthesis of multi-functional elastic polyaniline/polyvinyl alcohol composite gels by a solution assembly method. RSC Adv 10(37):22019–22026. https://doi.org/10.1039/d0ra02238a

[14] Pickering SU (1907) CXCVI.—Emulsions. J Chem Soc Trans 91:2001–2021. https://doi.org/10.1039/ct9079102001

[15] Fu EY, Chen KM, Wang QL, Zhang Y, Yan NN, Liu L (2021) Formation and stabilization of pickering emulsions using salt-sensitive core-shell cationic nanoparticles. J Mater Sci 56(25):14019–14034. https://doi.org/10.1007/s10853-021-06208-2

[16] Mi X, Wang XR, Gao CJ, Su WJ, Zhang YY, Tan XY, Gao JP, Liu Y (2019) Modified reduced graphene oxide as stabilizer for pickering w/o emulsions. J Mater Sci 55(5):1946–1958. https://doi.org/10.1007/s10853-019-04066-7

[17] Sun Z, Yan XX, Xiao Y, Hu LJ, Eggersdorfer M, Chen D, Yang ZZ, Weitz DA (2022) Pickering emulsions stabilized by colloidal surfactants: role of solid particles. Particuology 64:153–163. https://doi.org/10.1016/j.partic.2021.06.004

[18] Lu TT, Gou H, Rao HH, Zhao GH (2021) Recent progress in nanoclay-based Pickering emulsion and applications. J Environ Chem Eng 9(5):105941. https://doi.org/10.1016/j.jece.2021.105941

[19] Lyu W, Li JQ, Trchova M, Wang G, Liao YZ, Bober P, Stejskal J (2022) Fabrication of polyaniline/poly(vinyl alcohol)/montmorillonite hybrid aerogels toward efficient adsorption of organic dye pollutants. J Hazard Mater 435:129004. https://doi.org/10.1016/j.jhazmat.2022.129004

[20] Zhang B, Zhang TL, Zhang ZD, Xie MY (2019) Hydrothermal synthesis of a graphene/ magnetite/montmorillonite nanocomposite and its ultrasonically assisted methylene blue adsorption. J Mater Sci 54(16):11037–11055. https://doi.org/10.1007/s10853-019-03659-6

[21] Shin JH, Park JW, Kim HJ (2019) Clay-polystyrene nanocomposite from pickering emulsion polymerization stabilized by vinylsilane-functionalized montmorillonite platelets. Appl Clay Sci 182:105288. https://doi.org/10.1016/j.clay.2019.105288

[22] Yang ZY, Wang WX, Tai XM, Wang GY (2019) Preparation of modified montmorillonite with different quaternary ammonium salts and application in pickering emulsion.

New J Chem 43(29):11543–11548. https://doi.org/10.1039/c9nj01606f

[23] Li YF, Wen J, Xue ZZ, Yin XY, Yuan L, Yang CL (2022) Removal of Cr(VI) by polyaniline embedded polyvinyl alcohol/sodium alginate beads—extension from water treatment to soil remediation. J Hazard Mater 426:127809. https://doi.org/10.1016/j.jhazmat.2021.127809

[24] Rajendran S, Priya AK, Senthil Kumar P, Hoang TKA, Sekar K, Chong KY, Khoo KS, Ng HS, Show PL (2022) A critical and recent developments on adsorption technique for removal of heavy metals from wastewater-a review. Chemosphere 303(Pt 2):135146. https://doi.org/10.1016/j.chemosphere.2022.135146

[25] Jin LF, Huang L, Ren LL, He YJ, Tang JW, Wang S, Yang WC, Wang HY, Chai LY (2018) Preparation of stable and high-efficient poly(m-phenylenediamine)/reduced graphene oxide composites for hexavalent chromium removal. J Mater Sci 54(1):383–395. https://doi.org/10.1007/s10853-018-2844-9

[26] Pakade VE, Tavengwa NT, Madikizela LM (2019) Recent advances in hexavalent chromium removal from aqueous solutions by adsorptive methods. RSC Adv 9(45):26142–26164. https://doi.org/10.1039/c9ra05188k

[27] Mao W, Zhang Y, Luo JE, Chen LT, Guan YT (2022) Novel co-polymerization of polypyrrole/ polyaniline on ferrate modified biochar composites for the efficient adsorption of hexavalent chromium in water. Chemosphere 303(Pt3):135254. https://doi.org/10.1016/j.chemosphere.2022.135254

[28] Humpolicek P, Radaszkiewicz KA, Capakova Z, Pachernik J, Bober P, Kasparkova V, Rejmontova P, Lehocky M, Ponizil P, Stejskal J (2018) Polyaniline cryogels: biocompatibility of novel conducting macroporous material. Sci Rep 8(1):135–146. https://doi.org/10.1038/s41598-017-18290-1

[29] Hosseini H, Mousavi SM (2021) Bacterial cellulose/polyaniline nanocomposite aerogels as novel bioadsorbents for removal of hexavalent chromium: experimental and simulation study. J Clean Prod 278:123817. https://doi.org/10.1016/j.jclepro.2020.123817

[30] Chen J, Hong XQ, Zhao Y, Xia YY, Li DK, Zhang QF (2013) Preparation of flake-like polyaniline/montmorillonite nanocomposites and their application for removal of Cr(VI) ions in aqueous solution. J Mater Sci 48(21):7708–7717. https://doi.org/10.1007/s10853-013-7591-3

[31] Riahi Samani M, Ebrahimbabaie P, Vafaei Molamahmood H (2016) Hexavalent chromium removal by using synthesis of polyaniline and polyvinyl alcohol. Water Sci Technol 74(10):2305–2313. https://doi.org/10.2166/wst.2016.412

[32] Li JC, Li M, Wang S, Yang X, Liu F, Liu X (2020) Key role of pore size in Cr(VI) removal by the composites of 3-dimentional mesoporous silica nanospheres wrapped with polyaniline. Sci Total Environ 729:139009. https://doi.org/10.1016/j.scitotenv.2020.139009

[33] Han X, Liu YL, Xiong LJ, Huang HB, Zhang Q, Li L, Yu XH, Wei L (2019) Facile assembly of polyaniline/graphene oxide composite hydrogels as adsorbent for Cr(VI) removal. Polym Compos 40(S2):E1777–E1785. https://doi.org/10.1002/pc.25161

[34] Fan XX, Zhao BX, Ma JX, Wang N, Gao WQ, Gao YJ, Zhao YK, Liu LX (2022) Synthesis and characterization of magnetic organic montmorillonite: efficient adsorption of hexavalent chromium. Water Sci Technol 86(5):1135–1152. https://doi.org/10.2166/wst.2022.257

[35] Yu YR, Zhang G, Ye L (2019) Preparation and adsorption mechanism of polyvinyl alcohol/ graphene oxide-sodium alginate nanocomposite hydrogel with high Pb(II) adsorption capacity. J Appl Polym Sci 136(14):47318. https://doi.org/10.1002/app.47318

[36] Zhou TT, Liang QW, Zhou X, Luo HJ, Chen W (2021) Enhanced removal of toxic hexavalent chromium from aqueous solution by magnetic Zr-MOF@polypyrrole: performance and mechanism. Environ Sci Pollut Res Int 28(11):13084–13096. https://doi.org/10.1007/s11356-021-12341-x

[37] Li J, Yan LG, Yang YT, Zhang X, Zhu RX, Yu HQ (2019) Insight into the adsorption mechanisms of aqueous hexavalent chromium by EDTA intercalated layered double hydroxides: XRD, FTIR, XPS, and zeta potential studies. New J Chem 43(40):15915–15923. https://doi.org/10.1039/c9nj03479j

[38] Aarab N, Hsini A, Essekri A, Laabd M, Lakhmiri R, Albourine A (2020) Removal of an emerging pharmaceutical pollutant (metronidazole) using PPY-PANi copolymer: kinetics, equilibrium and DFT identification of adsorption mechanism. Groundw Sustain Dev 11:100416. https://doi.org/10.1016/j.gsd.2020.100416

[39] Yang DX, Li LF, Chen BL, Shi SX, Nie J, Ma GP (2019) Functionalized chitosan electrospun nanofiber membranes for heavy-metal removal. Polymer 163:74–85. https://doi.org/10.1016/j.polymer.2018.12.046

[40] González-López ME, Laureano-Anzaldo CM, Pérez-Fonseca AA, Arellano M, Robledo-Ortíz JR (2020) Chemically modified polysaccharides for hexavalent chromium adsorption. Sep Purif Rev 50(4):333–362. https://doi.org/10.1080/15422119.2020.1783311

[41] Tshemesea SJ, Mlabaa TT, Tichapondwaa SM, Mhike W (2020) Removal of chromium (VI) from aqueous solution using exfoliated graphite/ polyaniline composite. Chem

Eng trans 81:565–570. https://doi.org/10.3303/CET2081095

[42] Debnath MK, Rahman MA, Minami H, Rahman MM, Alam MA, Sharafat MK, Hossain MK, Ahmad H (2019) Single step modification of micrometer-sized polystyrene particles by electromagnetic polyaniline and sorption of chromium(VI) metal ions from water. J Appl Polym Sci 136(19):47524. https://doi.org/10.1002/app.47524

[43] Lai YX, Wang F, Zhang YM, Ou P, Wu PP, Fang QL, Chen Z, Li S (2019) UiO-66 derived N-doped carbon nanoparticles coated by PANI for simultaneous adsorption and reduction of hexavalent chromium from waste water. Chem Eng J 378:122069. https://doi.org/10.1016/j.cej.2019.122069

[44] Bao CZ, Chen MX, Liu GR, Jin X, Huang Q (2018) Efficient adsorption/reduction of aqueous hexavalent chromium using oligoaniline hollow microspheres fabricated by a template-free method. J Chem Technol Biotechnol 93(4):1147–1158. https://doi.org/10.1002/jctb.5473

[45] Luo YW, Wu ZL, Guan QH, Chen SX, Wu DS (2022) Facile synthesis of magnetic porous carbon nanosheets as efficient As(III) adsorbent. Chem Pap 76(12):7295–7303. https://doi.org/10.1007/s11696-022-02410-x

[46] Hsini A, Naciri Y, Benafqir M, Ajmal Z, Aarab N, Laabd M, Navio JA, Puga F, Boukherroub R, Bakiz B, Albourine A (2021) Facile synthesis and characterization of a novel 1,2,4,5- benzene tetracarboxylic acid doped polyaniline@ zinc phosphate nanocomposite for highly efficient removal of hazardous hexavalent chromium ions from water. J Colloid Interface Sci 585:560–573. https://doi.org/10.1016/j.jcis.2020.10.036

[47] Peng X, Yan ZC, Hu LH, Zhang RZ, Liu SJ, Wang AL, Yu XW, Chen L (2020) Adsorption behavior of hexavalent chromium in aqueous solution by polyvinylimidazole modified cellulose. Int J Biol Macromol 155:1184–1193. https://doi.org/10.1016/j.ijbiomac.2019.11.086

[48] Long FL, Niu CG, Tang N, Guo H, Li ZW, Yang YY, Lin LS (2021) Highly efficient removal of hexavalent chromium from aqueous solution by calcined Mg/Al-layered double hydroxides/polyaniline composites. Chem Eng J 404:127084. https://doi.org/10.1016/j.cej.2020.127084

[49] Das S, Chakraborty P, Ghosh R, Paul S, Mondal S, Panja A, Nandi AK (2017) Folic acid-polyaniline hybrid hydrogel for adsorption/reduction of chromium(VI) and selective adsorption of anionic dye from water. ACS Sustain Chem Eng 5(10):9325–9337. https://doi.org/10.1021/acssuschemeng.7b02342

[50] Hsini A, Benafqir M, Naciri Y, Laabd M, Bouziani A, Ez-Zahery M, Lakhmiri R, El Alem N, Albourine A (2021) Synthesis of an arginine-functionalized polyaniline@ FeOOH composite with high removal performance of hexavalent chromium ions from water: adsorption behavior, regeneration and process capability studies. Colloids Surf A Physicochem Eng Aspects 617:126274. https://doi.org/10.1016/j.colsurfa.2021.126274

[51] Lei C, Wang CW, Chen WQ, He MH, Huang BB (2020) Polyaniline@magnetic chitosan nanomaterials for highly efficient simultaneous adsorption and in-situ chemical reduction of hexavalent chromium: removal efficacy and mechanisms. Sci Total Environ 733:139316. https://doi.org/10.1016/j.scitotenv.2020.139316